Chalcogenide coatings of $Ge_{15}Sb_{20}S_{65}$ and $Te_{20}As_{30}Se_{50}$

Virginie Nazabal,[1,*] Michel Cathelinaud,[2,*] Weidong Shen,[2] Petr Nemec,[3] Frédéric Charpentier,[1]
Hervé Lhermite,[4] Marie-Laure Anne,[1] Jérémie Capoulade,[2] Fabien Grasset,[1] Alain Moreac,[5]
Satoru Inoue,[6] Miloslav Frumar,[3] Jean-Luc Adam,[1] Michel Lequime,[2] and Claude Amra[2]

[1]Sciences Chimiques de Rennes, UMR 6226, Université Rennes 1, 35042 Rennes, France
[2]Institut Fresnel, UMR 6133, CNRS, Ecole Centrale Marseille, Université Paul Cezanne Aix Marseille, Université de Provence,
13397 Marseille, France
[3]Department of General and Inorganic Chemistry, Faculty of Chemical Technology, University of Pardubice,
Legions Square 565, 53210 Pardubice, Czech Republic
[4]Institut d'Electronique et de Télécommunications de Rennes-Microelectronic, Université Rennes 1,
35042 Rennes, France
[5]Groupe Matière Condensée et Matériaux, UMR 6626, Université Rennes 1, 35 042 Rennes Cedex, France
[6]National Institute for Materials Science, 1-1 Namiki, Tsukuba, 305-0041, Japan

*Corresponding author: michel.cathelinaud@fresnel.fr; virginie.nazabal@univ-rennes1.fr

Chalcogenide coatings are investigated to obtain either optical components for spectral applications or optochemical sensors in the mid-infrared. The deposition of $Ge_{15}Sb_{20}S_{65}$ and $Te_{20}As_{30}Se_{50}$ chalcogenide glasses is performed by two physical techniques: electron-beam and pulsed-laser deposition. The quality of the film is analyzed by scanning electron microscopy, atomic force microscopy, and energy dispersive spectroscopy to characterize the morphology, topography, and chemical composition. The optical properties and optical constants are also determined. A CF_4 dry etching is performed on these films to obtain a channeled optical waveguide. For a passband filter made by electron-beam deposition, cryolite as a low-refractive-index material and chalcogenide glasses as high-refractive-index materials are used to favor a large refractive-index contrast. A shift of a centered wavelength of a photosensitive passband filter is controlled by illumination time. © 2008 Optical Society of America

OCIS codes: 120.4530, 160.4760, 310.0310, 310.3840, 160.4670.

1. Introduction

Chalcogenide glasses are transparent in the near- and mid-infrared regions of the spectrum ($0.5–10\ \mu m$ for sulfides, $0.8–12\ \mu m$ for selenides, and up to $20\ \mu m$ for tellurides) and present high refractive indices, typically in the range of $2.0–2.9$ at $1.5\ \mu m$ [1]. They have been applied as optical materials in this region (lenses, coatings, prisms, plates, filters). They also present attractive properties for a nonlinear optical field. It is well established that $\chi^{(3)}$ of chalcogenide glasses is approximately 2 orders of magnitude larger than that of silica, and large second-harmonic generation (SHG) efficiencies can be expected in such glasses.

In addition, these amorphous chalcogenides can be deposited in thin films as optoelectronic components [2,3]. With their specific physicochemical properties, these materials can also be used in optical coatings, such as bandpass filters for telecommunication or spatial applications in the infrared range. In another field, optochemical sensors with complex planar structures can make use of chalcogenide films for exploring the IR spectral domain [4–7]. Mid-IR optic sensors are of great interest with their inherent molecular selectivity, allowing qualitative and quantitative analysis of various chemical and biological species [8,9].

Moreover, chalcogenide amorphous films can see their absorption edge shifted either toward longer or shorter wavelengths (photodarkening and photobleaching, respectively) and their refractive indices modified under light irradiation of appropriate en-

ergy and intensity. The photoinduced effects of chalcogenide glasses and films are related to modification of their electronic and atomic structure and their physicochemical properties. This behavior strongly depends on the choice of chemical system, composition, and deposition method. Consequently, the photoinduced refractive-index variation of chalcogenide films could be exploited for selective channel writing or Bragg gratings in a planar waveguide [10–13] or laser trimming of interference filters [14,15].

In this work, we are interested in two chalcogenide films of composition $Ge_{15}Sb_{20}S_{65}$ and $Te_{20}As_{30}Se_{50}$, called 2S1G and TAS, respectively. These particular compositions were chosen because of their remarkable properties: large optical window covering the spectral region from 500 nm to 11 μm for 2S1G and from 1.3 to 18 μm for TAS, excellent resistance to devitrification, suitable durability toward water and solvent corrosion, and high refractive index. Moreover, in the case of 2S1G, photosensitivity was reported in the system of Ge–Sb–S [16]. We investigate the chalcogenide film deposition by two deposition methods: electron-beam deposition (EBD) and pulsed-laser deposition (PLD). The PLD method is promising for preparation of thin films of complex composition because all components of the target can be evaporated at once [17]. The EBD presents the advantage of being able to deposit homogeneous thick and large size films. Each method having advantages and disadvantages, the comparison of the resulting films from targets with identical starting compositions is significant, making our purpose successful.

2. Experimental Methods

A. Glass Target Synthesis

The chalcogenide glasses of composition $Ge_{15}Sb_{20}S_{65}$ and $Te_{20}As_{30}Se_{50}$ are prepared in the form of rods from the appropriate amounts of high-purity commercial elements (99.999%): As, S, Se, and Te, specially purified to remove oxygen, molecular water, carbon, and silica. These impurities introduce absorption in the mid- and far-IR ranges, as well as scattering losses due to microinclusions. The chemical reagents S and Se are purified by vacuum distillation with a low rate of evaporation. The synthesis reactor is evacuated in an oil-free vacuum (10^{-4} mbar). Then, the sealed ampoule containing the reagents is placed into a rocking furnace heated at 850 °C for 12 h for 2S1G (650 °C for 8 h for TAS) and quenched in water. In the final stage, samples are annealed at a temperature near Tg (the glass transition temperature) for 4 h and cooled slowly to room temperature. The glass samples are obtained as rods with a diameter of 18 mm for EBD and 25 mm for PLD with a length of approximately 50 mm. Several glass cylinders are obtained from the same batch, allowing great reproducibility between successive depositions and also for the PLD and EBD deposition methods, which use exactly the same bulk batch. For optical characterization, bulk samples of 1 mm thickness are polished with fine powders of dimensions up to 0.5 μm to obtain flat surfaces and parallel sides.

B. Deposition and Photolithographic Processes

Typical equipment for EBD used for the preparation of coatings is a Balzers BAK 600 evaporation plant with a 60 cm stainless steel bell jar, equipped with two electron-beam guns with water-cooled crucibles. The chalcogenide materials are placed in an intermediate graphite liner of 4 cc capacity. An x–y sweep can be applied to the electron beam, and it can be adjusted to evaporate a relatively large area, increasing the film uniformity. The films are deposited on the fused-silica or silicon substrates that are subjected to a normal cleaning procedure before being cleaned by a discharge in a vacuum chamber.

Controlled by a quartz-crystal monitor, deposition took place at a rate of 1 nm/s with a pressure of the order of 2.10^{-6} mbar. Optical monitoring in transmission was used to control the manufacturing of single layers and passband filters. For all coatings, we used colored glass filters to avoid the influence of light absorption during the deposition due to the bandgap energy of the materials located in the visible spectral range (Schott OG 550 and RG 830, respectively, for 2S1G and TAS). To follow the coating formation in real time, suitable wavelengths of approximately 840 and 1550 nm were selected, respectively, for 2S1G and TAS [18,19].

For the manufacturing process of the passband filter, zinc sulphide (ZnS) and cryolite (Na_3AlF_6) were selected to perform the mirror parts considering that the parameters of evaporation are compatible with those of chalcogenide glasses, particularly for the TAS composition. These materials deposited at ambient temperature for the substrates are well known for their use as high- or low-refractive-index (2.25 and 1.35 at 1.5 μm for ZnS and Na_3AlF_6, respectively) materials with the EBD technique [20].

For PLD, a KrF excimer laser operating at 248 nm with a constant output energy of 200 mJ per pulse, with a pulse duration of 30 ns, and operating at 20 Hz was used. The laser energy incident on the target surface was fixed at 1.4 J.cm^{-2}. Thin films were deposited in a vacuum chamber with a residual pressure of 2.10^{-6} mbar before each experiment on substrates held at room temperature. The target-to-substrate distance was approximately 5 cm with rotating substrates. To limit damage to the surface upon laser irradiation, a laser beam translation made it possible to scan the target surface, leading to a uniformly ablated surface of 1×1.2 cm area. For the considered laser energy, the deposition rates were approximately 0.8 and 0.6 nm/s for TAS and 2S1G, respectively.

A classical photolithography process was used to prepare dry etching with a positive (S1813) or negative (SU8 2002) photoresist. First, the photoresist is spin coated on the wafers. After a soft bake, the photoresist is then exposed through a Cr mask thanks to an i-line mask aligner. After a postexposure bake, the

exposed bands (positive photoresist) or nonexposed bands (negative photoresist) were dissolved with a suitable developer. The experimental setup used for reactive physical ion etching consists of a Nextral radio frequency sputtering with CF_4 gas since the F^- ions were suitable to form volatile species with chalcogenide elements. After a hard bake, waveguides were etched with a gas flux from 10 to 30 SCCM (SCCM denotes cubic centimeters per minute at standard temperature and pressure) under gas pressure between 3 and 10 mTorr and with a RF power range of approximately 30–100 W. This process allows a good etching uniformity. The etch rate of TAS and 2S1G is approximately 200 nm/min. A number of rib waveguides were fabricated with widths from 3 to 400 μm and etch depths from 0 to 3 μm.

C. Bulk and Film Characterization

For optical properties, chemical composition, structure, topography, and morphology investigation, silicon and silica substrates were placed in the deposition chambers for the PLD and EBD techniques.

The composition of bulk glass and films was measured using a scanning electron microscope (SEM) with an energy-dispersive x-ray analyzer (JSM 6400-OXFORD Link INCA), and the morphology of the film was observed by a field-emission gun SEM (JSM 6301F). For the case of the observation of morphology and the composition of the multilayer, we used a high-resolution field-emission SEM (Hitachi-S4800) including energy-dispersive x-ray spectroscopy (Horiba 7593-H).

Raman spectra were measured using a Ti:sapphire tunable laser (Spectra-Physics 3900S, exciting line at 748 nm for this study) coupled to a confocal micro-Raman triple spectrometer (DILOR XY500) in backscattering configuration; the typical resolution was 2.5 cm^{-1}. All spectra were recorded at room temperature.

The surface roughness of the layers was measured with an atomic force microscope (Quesant Q-scope 250). We used contact mode imaging with a scanned area of 2×2 μm in general.

Thermal analysis, with an accuracy of ± 2 °C for determination of Tg, was performed on a differential scanning calorimeter (TA Instruments DSC 2010) with a heating rate of 10 °C/min, and the typical sample weight was approximately 10 mg. The density was measured in CCl_4 using the Archimedes principle with an accuracy of ± 0.005 g/cm^3. The density and glass transition temperature of the chalcogenide glasses used are 3.2 and 250 °C for the 2S1G and 4.5 and 137 °C for the TAS.

The transmittance and reflectance of the bulk glass and thin chalcogenide films were measured using visible–near-infrared and Fourier transform infrared spectrophotometers. In the 320–900 and 600–1700 nm spectral regions, a PerkinElmer 18 and a fiber spectrophotometer (with a typical resolution of 5 nm and sample analysis area of 1 mm^2 for mapping) were used, respectively [21]. In the case of the films

deposited on a fused-silica substrate, a determination of optical constants has been performed on a large spectral range through reflectance and transmittance measurements and with a variable angle spectroscopic ellipsometer (VASE, J.A. Woollam Co., Inc.). Ellipsometric measurements allowed a spectral range extension from 500 to 2300 nm at three different angles of incidence of the primary light beam (65°, 70°, and 75°). In the case of the photosensitivity characterization of the single layers and passband filter, a tunable laser diode was used in the spectral range of 1520–1570 nm. The effective refraction indices of the propagation modes in the planar waveguide were measured with a Metricon-2010 instrument . A laser beam at wavelengths of 1302 and 1540 nm for both TE and TM polarization and a silicon prism were used to excite the TE and TM modes inside the planar chalcogenide waveguides [22].

3. Experimental Results

A. Chalcogenide Optical Results

The transmittance of TAS and 2S1G bulk glasses with a thickness of approximately 1 mm is shown in Fig. 1. The refractive indices of the glass targets in the contact zone obtained from the prism-coupling configuration are 2.38 and 2.98 for 2S1G and TAS at 1.54 μm, respectively. The transmittance of TAS and 2S1G thin films deposited by PLD and EBD for several thicknesses (Figs. 2a and 2b) proves that the layers obtained by these deposition methods present, on the whole, good optical qualities. The transmittance of 2S1G and TAS EBD was recorded for three thicknesses (1.2 and 1.7 μm, respectively, and 5 μm) and compared with a PLD thin film. For 2S1G, a bandgap energy shift is observed between the PLD and EBD films. In the case of TAS PLD film, such a shift is not present, but a reduction of oscillation amplitude of the transmittance can be noted. This behavior could have its origins in the inhomogeneous and more absorbent layer obtained by PLD compared with that obtained by EBD.

According to the literature [23,24], the refractive index and the thickness of the film can be determined
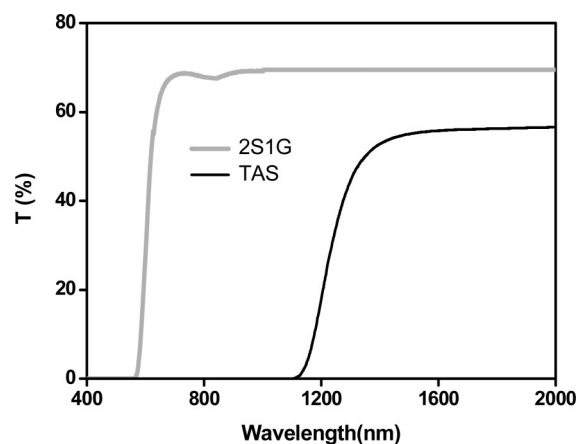

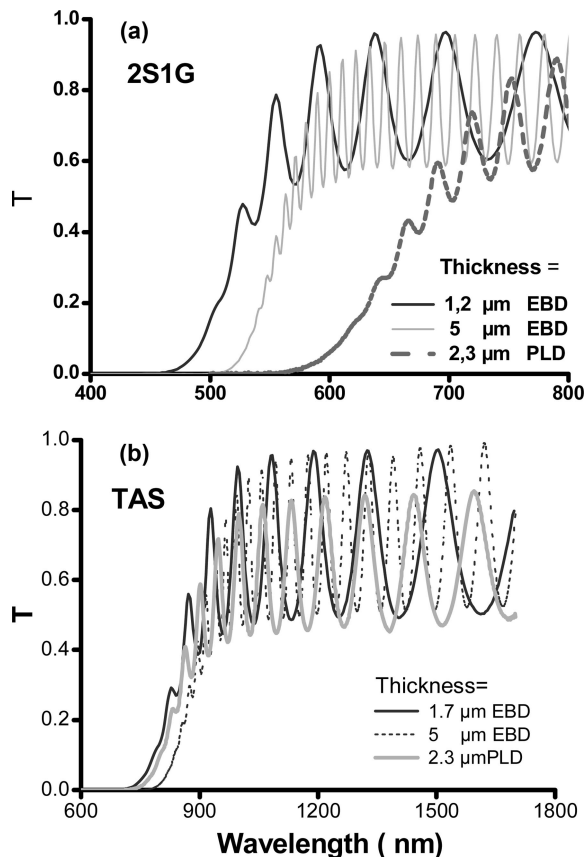Fig. 1.   Transmission of TAS and 2S1G bulk.

Fig. 2. Transmission of (a) 2S1G and (b) EBD films obtained by PLD or EBD for several thicknesses deposited on silica substrates.

Fig. 3. Refractive index dispersion curves of 2S1G and TAS EBD films obtained by VASE ellipsometry and spectrophotometry.

starting from the transmittance and reflectance curves. Considering this refractive-index method, the films obtained by EBD and PLD are homogeneous, except in the case of the TAS PLD films, which are also absorbent ($k = 0.003$ at 1550 nm). In comparison, for the refractive index and the thickness of the film measured by VASE, the experimental data were fitted using a classical Cauchy dispersion law. The values obtained by these first two optical methods are presented in Fig. 3, whereas the third method used, the M-lines technique [25,26], gives the optogeometric parameters of several films (Fig. 4). By comparison, some classical differences appear [27], which depend on the model used and accuracy measurements, but the agreement between these various optical characterization methods is satisfactory.

At 1540 nm, far from the absorption edge, the refractive index is equal to 2.42 ± 0.01 for 2S1G and 2.87 ± 0.01 for TAS EBD films with a thickness of 1.55 μm, which is in good agreement with the refractive indices of bulk samples. A decrease in refractive index seems to be related to an increase in film thickness with $\Delta n_{2SIG} = 0.02$ and $\Delta n_{TAS} = 0.01$ obtained by ellipsometry for a thickness variation of approximately 3 μm, considering the measurement accuracy. These slight variations of the refractive index, as a dependence of the thickness, can be explained by lower uniformity of the thick film (5 μm) obtained

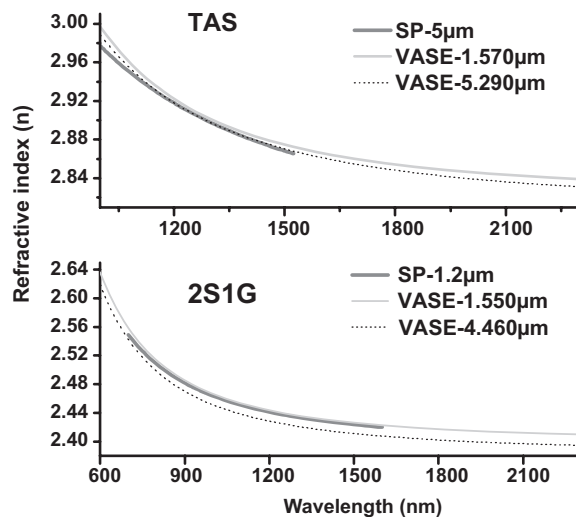after several hours of deposition. It is well known that as a result of irradiation and/or thermal annealing of chalcogenide films, many of their properties are changed; in particular, a shift of the bandgap absorption and also a refractive-index variation can be observed [28]. Thus, during the deposition, the variations of temperature (approximately 20 °C) in the chamber and electronic bombardment power (5%) during EBD can also play a role in the layer quality.

Whatever the film thickness, the high-refractive-index value of the chalcogenide films is associated with a very low absorbance in the NIR part of the spectrum ($k < 10^{-4}$), and especially in the telecommunication C-band, around 1550 nm, except for TAS PLD film.

The refractive indices of samples obtained by PLD are generally a little bit lower than those for the films obtained by EBD. For instance, the PLD films with an intermediate thickness (2.6 and 3.1 μm) have comparable values, as determined by spectrophotom-
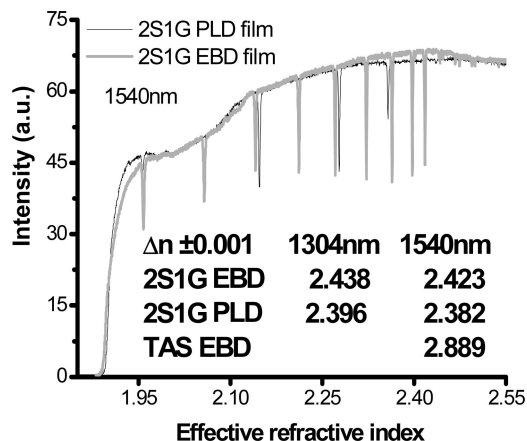

Fig. 4. M-lines with Si prism-coupling configuration at 1540 nm for 2S1G PLD and EBD films and indices of refraction of 2S1G PLD and EBD films and TAS EBD film.

etry at 1.5 μm, to EBD thick film (5 μm). This slight difference can be explained by the fact that the deposition techniques do not exactly employ the same physical processes, mainly due to divergence in terms of energy used for evaporation [17]. Thus, an analysis of the chemical composition and structural investigation by Raman scattering was carried out on the films compared with bulk targets to extend the scope of the investigation for a better understanding of the processes involved.

B.   Characterization of Chalcogenide Pulsed-Laser and Electron-Beam Deposition Films: Composition, Structure, Topography, and Morphology

To understand the observations obtained by optical methods, studies were undertaken on the chemical composition, structure, topography, and morphology of these films. During the evaporation process, the effective temperature of vapors is relatively high and chalcogenides can dissociate into fragments containing more- and less-volatile species. The disorder and composition range of amorphous chalcogenide is important with a large free volume available. These characteristics are beneficial for the formation of compositional and coordination defects, which can play a large part in optical properties (bandgap energy, refractive index, photosensitivity, etc.), all the more in amorphous films. As a result, their composition and structure are strongly influenced by the deposition conditions and can be investigated by energy dispersion and Raman scattering spectroscopy, respectively.

The analysis of EBD and PLD films by EDS allows the determination of their chemical composition of the various elements deposited on silicon. The film composition was compared with those theoretical and real of the $Ge_{15}Sb_{20}S_{65}$ and $Te_2As_3Se_5$ synthesized bulk glasses. Table 1 sums up the analysis results. For the 2S1G films, the chemical composition obtained by EBD is close to bulk material, except a low deficiency of sulphur (3%) usually observed for sulphide film deposition. Contrary to EBD 2S1G film, the deposition by PLD with an energy fluency of 1.4 J/cm^2 causes a substantial loss of sulphur, which increases the proportion of (semi-)metal in the films and also the relative proportion of antimony in comparison with germanium. This analysis can explain

the difference observed on optical bandgap energy for EBD and PLD film with a shift of transmittance toward the NIR wavelengths (Fig. 2a). In the case of TAS film, the variation of refractive index between EBD and PLD films cannot be explained by a simple variation of the composition, which is really close (with regard to EDS accuracy, ±0.5 %) to that of a bulk glass target (Table 1).

On the Raman scattering spectrum of 2S1G glass (Fig. 5a), a main large vibration band is present in the range of 265 and 365 cm^{-1}. This large band can be decomposed into two main bands, considering the composition of the glass. One band located close to 335 cm^{-1} can be associated with the ν_1 symmetric stretching mode of [GeS$_4$] tetrahedrons [29], and the presence of antimony induces the appearance of a vibration band at approximately 295 cm^{-1} associated with the vibration of the [SbS$_3$] trigonal pyramids [30,31]. The other peaks usually related to the medium range order structure of GeS$_2$ have been attributed to ν_{1c}, usually called the companion peak, whose origin remains controversial, and to the vibration of Ge–S bonds in tetrahedral units linked by corners, [29,32]. Moreover, because of the nonstoichiometry of the glass, the small band related to the vibration of the S–S bonds is also observable at 476 cm^{-1} on Raman spectra, which can be related to the connection of two tetrahedral or trigonal units by two sulfur atoms [33]. The Raman spectra of the PLD and EBD films are also mainly dominated by the band located between 265 and 365 cm^{-1}, which overlaps the symmetric stretching modes of both [GeS$_4$] tetrahedrons and [SbS$_3$] trigonal units. For PLD film, the relative intensity between these two bands seems to change to the profit of the band associated with antimony, which is in agreement with the composition of the film. It is also marked by the appearance of two new bands of vibration at 165 and 208 cm^{-1}, which can be connected with vibrations of metal bonds such as Sb–Sb bonds for the first peak [30,31] and Ge–Sb- and/or Ge-based tetrahedral structural units containing fewer than four S atoms for the second peak (GeS$_3$Ge, GeS$_2$Ge$_2$, etc.) [29].

For TAS samples (Fig. 5b), the Raman spectra present two main peaks and one important shoulder at 170, 205, and 238 cm^{-1}, respectively. The nominal composition of the glass (As$_{30}$Se$_{50}$Te$_{20}$) presents an excess of Se and Te compared with the As$_{40}$(Se, Te)$_{60}$ stoichiometric composition that can promote the formation of Te–Te, Se–Te, or Se–Se bonds, which can connect the pyramidal units of arsenic. Raman spectra of an As–Se system present a broad main band in the region of 200–300 cm^{-1} [34]. In the case of As$_{40}$Se$_{60}$ glass, the peak position of the main broad band is located at 240 cm^{-1}, which is connected with the stretching vibration modes of [AsSe$_3$] pyramidal units. Consequently in the Raman spectra of TAS, the shoulder at 238 cm^{-1} can be related to the vibration of [AsSe$_3$] units keeping in mind that a contribution may come from the formation of Se–Se in Se$_n$ chains [35]. The extension of the band to 260 cm^{-1}

Table 1.   Chemical Composition by EDS of 2S1G and TAS Bulk Glass and PLD and EBD Films

Element	Theoretical (at. %)	Bulk (at. %)	EBD Film (at. %)	PLD Film (at. %)
2S1G				
Ge	15	14.8	15.3	15.1
Sb	20	21.0	22.5	26.8
S	65	64.2	62.2	58.1
TAS				
Te	20	20.5	19.8	21.3
As	30	29.5	30.9	28.4
Se	50	50.0	49.3	50.3

Fig. 5. Raman scattering spectra of (a) 2S1G and (b) TAS bulk glass and EBD and PLD films.

pared by thermal evaporation, it appears at approximately 173 cm^{-1} in samples with compositions of approximately $x = 0.3$ [36].

Finally and in a first approach, the network structure of the 2S1G EBD film is close to that of bulk glass, considering the Raman and EDS analysis. It can be described as [GeS$_4$] tetrahedral and [SbS$_3$] pyramidal units connected by sulphur and by some S–S bridges, respecting the small sulphur excess of approximately 5%. This conclusion cannot be applied to PLD film for which the formation of defect bonds is encouraged by the formation energies of a metal homopolar bond not far from the heteroatomic bond (GeS or SbS) energies. These structural results have repercussions for the optical properties of the 2S1G films, which are comparable with bulk glasses for EBD film but further apart for PLD films. In the case of TAS composition, it is important to note that no important discrepancy between bulk glass and film occurs. The composition of PLD and EBD films are really close to that of the bulk glass target, and film networks seem not to be really modified by the deposition. The TAS network seems to be mainly composed of [AsSe$_3$] connected by Se and bridges of Se–Se and Se–Te due to the excess of chalcogens (55%). The formation of Te–Te seems to occur, but it is difficult not to consider the formation of As–Te, considering the comparable value of their bond energy [17].

For topography measurements obtained by AFM, we used TAS and 2S1G films deposited on silica substrates. The root-mean-square (rms) roughness estimated from AFM images measured over an area of 2 μm $\times$ 2 μm is approximately the same for the 2S1G films by PLD and EBD deposited on a silica substrate of approximately 0.91 and 0.97 nm, respectively
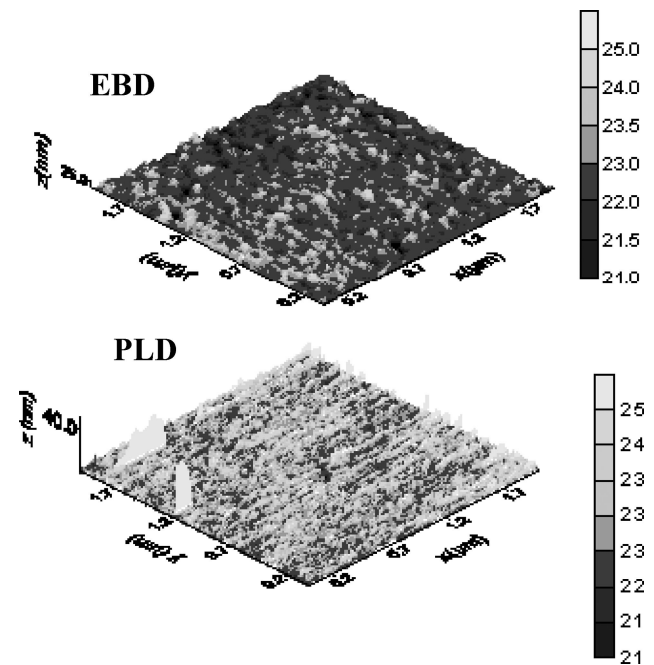

Fig. 6. AFM picture of 2S1G PLD and EBD films on fused-silica substrate (mapping of 2 μm $\times$ 2 μm).

could be related to the formation of Se–Se to form As–Se–Se–As. For the band at 200 cm^{-1}, this line has been assigned to vibrations of neighboring Se–Te bonds [36]. The band at 170 cm^{-1} should be related with Te–Te or less probably Te–As. Effectively, according to literature, two bands at 155 and 182 cm^{-1} have been recorded in As$_{50}$Te$_{50}$ glass, and the first was associated with Te–Te bond vibrations [37]. In the case of amorphous Se$_{1-x}$Te$_x$ thin-film alloys, pre-

(Fig. 6). A similar study for the TAS shows a clear difference between coating techniques. Indeed, the roughness is 95 nm for PLD compared with 0.8 nm obtained with the EBD method. Nevertheless, between these nodules defined as microinclusions, roughness is rather low (0.4 nm). This strong roughness is explained by the appearance of nodules irregularly spaced on the surface of the PLD film. A well-known disadvantage of the PLD method is the possible presence of particulates (droplets) in the deposited films. These nodules form light-scattering sites, resulting in the optical quality of the films being lowered, explaining the difference observed on transmission. These nodules also explain why the layer cannot be regarded as homogeneous film, affecting also the determination of the refractive index by the M-lines technique.

The TAS and 2S1G films were deposited on silicon and directly cleaved for a morphology characterization by a SEM (Fig. 7). An amorphous structure for the 2S1G films is observed, whatever the deposition technique used, with neither columnar nor granular microstructure (Figs. 7a and 7b). The film microstructure can be considered vitreous—according to criteria de-
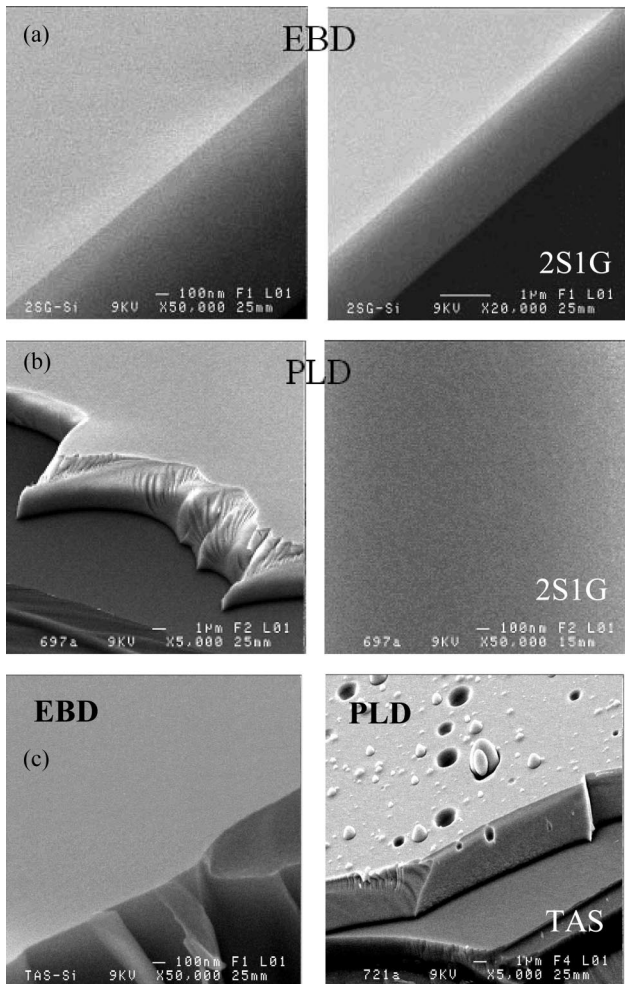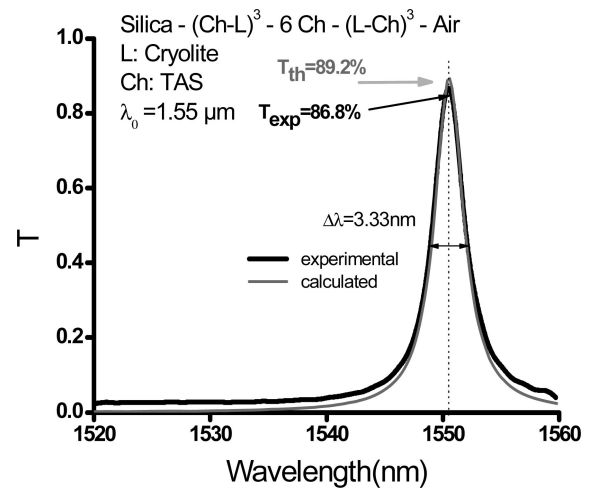

Fig. 8. Experimental and theoretical transmittance of a TAS/cryolite passband in the spectral range of a tunable laser (1520–1570 nm).

fined by Guenther *et al.* [38]—and so the packing density should be near 1. The microstructure of the TAS PLD films is, as expected from AFM analysis, made of nodules of approximately 100 nm to 1 μm with a smooth area between them (Fig. 7c). In the case of EBD films, free from cleavage defect consideration, the layer is amorphous, and not porous, as 2S1G film.

C. Passband Filter

Since all EBD layers have undergone an adhesion test with success [39], the selected TAS and 2S1G glasses were used to confirm the potentiality offered by chalcogenide glass as a high-refractive-index material and a spacer layer of an all-dielectric passband Fabry–Perot filter centered at 1550 nm and described by the following formulas: $Silica - (Ch\text{-}L)^n - pCh - (Ch\text{-}H)^n - Air$ and $Silica - (H\text{-}L)^n - pCh - (L\text{-}H)^n - Air$ in which L is a low-index quarter-wavelength cryolite layer and the notation Ch is a 2S1G or TAS high-
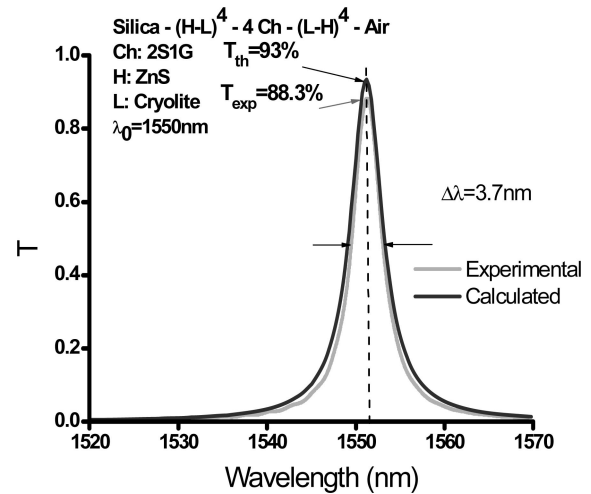

Fig. 9. Transmittance of a passband in the spectral range of a tunable laser (1520–1570 nm).

Fig. 7. SEM images of 2S1G and TAS films deposited by EBD and PLD on silicon substrate.

index layer, where $(Ch-L)^n$ or $(H-L)^n$ describe the classical periodical alternations of quarter-wavelength mirrors. To obtain a good rejection ($R \approx 96\%$) for mirrors $(H-L)^n$ and $(L-H)^n$, the degree n must be included between three and four; the index p of the quarter-wavelength of the spacer is included between four and six to obtain a relatively narrow bandwidth FWHM, near 3 nm, at 1550 nm. To manufacture these optical coatings and compensate the intrinsic photosensitivity effects, the optical monitoring allows the optical thickness to be adjusted for each layer at the centered wavelength. Transmittance recorded in the spectral range of 1520–1570 nm (Figs. 8 and 9) shows good agreement with the theoretical prediction. These first results prove the compatibility of zinc sulphide and cryolite as classical materials with glass chalcogenide as a new material to obtain optical coatings. The slight differences observed can be ex-

plained by three main causes: bulk scattering of ZnS and cryolite layers, uniformity since a small crucible area was used to deposit cryolite and chalcogenides, and/or interface problems. To better understand the slight difference between the theoretical and experimental results, in the particular case of the filter Silica $-$ $(Ch-L)^3$ $-$ $6Ch$ $-$ $(L-Ch)^3$ $-$ Air, the SEM images of the cross section of this coating deposited on silicon was carried out. Figure 10 reveals the amorphous character of the TAS, identical to the single layer study and crystalline character of cryolite made of nanocrystallites (≤ 100 nm), which is considered a porous material. The chemical composition of this coating is in good agreement with the TAS single-layer analysis, in spite of the difficulty of extracting chemical composition directly on a cross section of the filter.

D. Applications and Photoinduced Effect

As mentioned in the introduction, this study was motivated by the need for an accurate characterization (chemical composition, morphology, refractive index) of the selected 2S1G and TAS chalcogenide films in order to manufacture optical components likely to present a photoinduced effect. Such optical components are of great interest, in particular to detect gas in the mid-IR or for telecommunication applications in the C-band. As applications of this study of chalcogenide thin films, we present briefly in this subsection, our principal experimental achievements. Under these conditions, a broadband light illumination was carried out on a single layer and a passband filter with a spacer made of 2S1G and TAS, resulting in a shift of more than 5 nm in the central resonant wavelength toward the short and long wavelengths, respectively. The shift of the centered wavelength at 1552 nm of a passband filter made of TAS and cryolite according to the influence of the time of local illumination is reported in Fig. 11. The photodarkening observed in this case could be related to the formation of defects and localized electronic states in the tails of conduction and valence bands, which lower the energy gap. The chalcogens (S, Se) and pnictogens
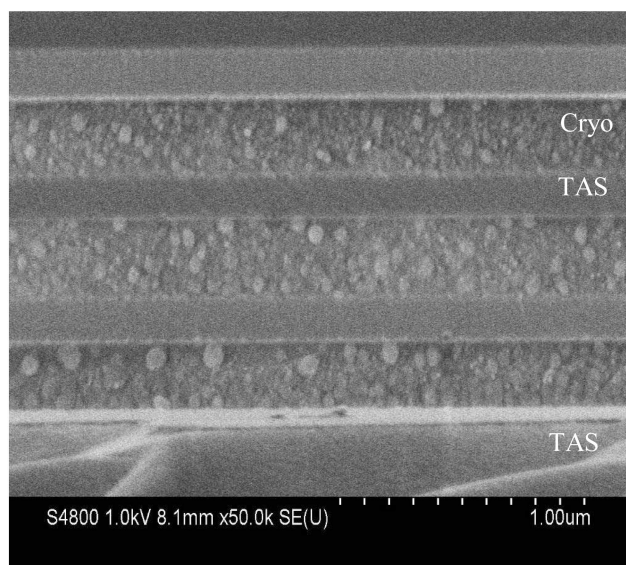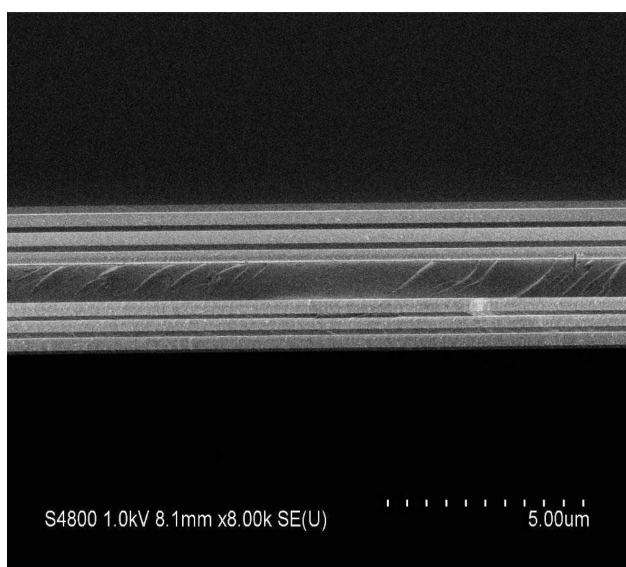

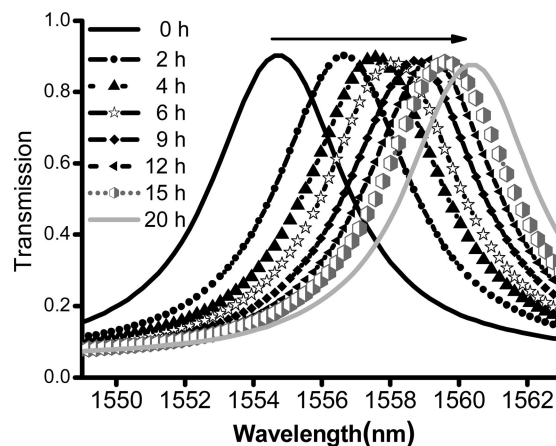Fig. 10. SEM image of a cross-section passband filter: Silica $-$ $(Ch-L)^3$ $-$ $6Ch$ $-$ $(L-Ch)^3$ $-$ Air.

Fig. 11. Local illumination effect on the centered wavelength for a passband filter: Silica $-$ $(Ch-L)^3$ $-$ $6Ch$ $-$ $(L-Ch)^3$ $-$ Air.
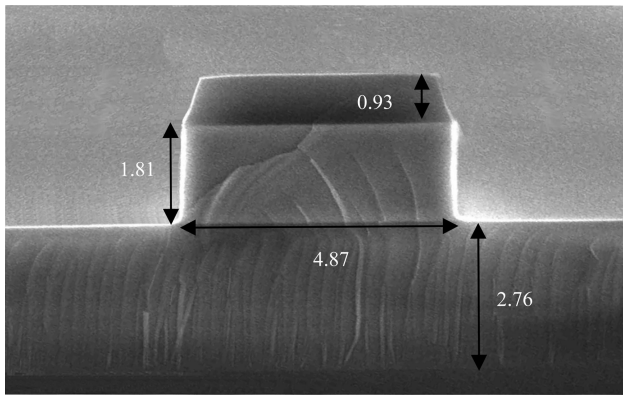
Fig. 12. SEM image showing rib waveguide of TAS deposited by EBD made by CF_4 dry etching.

(As, Sb), which are in large proportion in the selected chalcogenide glasses, can take part in the photoinduced effect with their nonbonding orbitals (lone pairs) forming the upper part of valence band states and favored by the presence of chalcogen in the excess developing bridge, as shown by Raman scattering spectroscopy [40].

For optical integrated applications apart from the use of photosensitivity to increase the refractive index, which presents some drawbacks, lateral confinement of light can be performed on chalcogenide by dry etching [41,42]. Ribs of 0.1 to 2 μm in depth were obtained on PLD and EBD films using a CF_4 gas. The ribs are well resolved as shown by a SEM on TAS EBD film (Fig. 12). Thus, TAS and 2S1G waveguides with vertical and relatively smooth sidewalls were obtained, and the film roughness was low enough to forecast having suitable optical losses (<1 dB/cm at 1.55 μm for 2S1G [43]) for microsensor or nonlinear optical application.

4. Conclusion

The deposition of $Ge_{15}Sb_{20}S_{65}$ and $Te_{20}As_{30}Se_{50}$ chalcogenide glasses (2S1G and TAS) has been performed by two physical techniques: pulsed-laser and electron-beam deposition. The quality of the films was analyzed by nonoptical methods (SEM, EDS, AFM) and by optical methods to determine their optical constants. A dissimilarity of these characteristics between PLD and EBD films was highlighted, and the quality of the TAS PLD film should be improved by varying the deposition parameters. A CF_4 dry etching was performed for TAS and 2S1G film. This anisotropic etching could allow a lateral confinement of the light in optic sensor fabrication or nonlinear optic application. 2S1G and TAS waveguides with vertical and relatively smooth sidewalls were obtained, allowing the forecasting of suitable scattering losses for EBD film or improved PLD film. For coatings, and in particular for passband filters, we have used cryolite as a low-refractive-index material and chalcogenides as high-refractive-index materials for manufacturing with the EBD technique, favoring a large refractive-index contrast.

The wide range of photoinduced phenomena exhibited by chalcogenide glasses enable them to be used in a variety of optical applications. A particularly important feature of some of these phenomena is their ability to change the refractive index of chalcogenide glasses. Thus, the photosensitivity has repercussions for the centered wavelength shift of a passband filter controlled by illumination time. These changes could take an interesting role in the fabrication of integrated optical components and devices such as selective optical filters, couplers, and modulators.

References

1. S. R. Elliott, *Physics of Amorphous Materials* (Longman, 1990).
2. A. K. Mairaj, A. M. Chardon, D. P. Shepherd, and D. W. Hewak, "Laser performance and spectroscopic analysis of optically written channel waveguides in neodymium-doped gallium lanthanum sulphide glass," IEEE J. Sel. Top. Quantum Electron. **8**, 1381–1388 (2002).
3. V. G. Ta'eed, M. Shokooh-Saremi, L. B. Fu, I. C. M. Littler, D. J. Moss, M. Rochette, B. J. Eggleton, Y. L. Ruan, and B. Luther-Davies, "Self-phase modulation-based integrated optical regeneration in chalcogenide waveguides," IEEE J. Sel. Top. Quantum Electron. **12**, 360–370 (2006).
4. N. Ho, M. C. Phillips, H. Qiao, P. J. Allen, K. Krishnaswami, B. J. Riley, T. L. Myers, and N. C. Anheier, "Single-mode low-loss chalcogenide glass waveguides for the mid-infrared," Opt. Lett. **31**, 1860–1862 (2006).
5. J. Hu, V. Tarasov, A. Agarwal, L. Kimerling, N. Carlie, L. Petit, and K. Richardson, "Fabrication and testing of planar chalcogenide waveguide integrated microfluidic sensor," Opt. Express **15**, 2307–2314 (2007).
6. A. Ganjoo, H. Jain, C. Yu, R. Song, J. V. Ryan, J. Irudayaraj, Y. J. Ding, and C. G. Pantano, "Planar chalcogenide glass waveguides for IR evanescent wave sensors," J. Non-Cryst. Solids **352**, 584–588 (2006).
7. C. Vigreux-Bercovici, L. Labadie, J. E. Broquin, P. Kern, and A. Pradel, "Selenide and telluride thick films for mid and thermal infrared applications," J. Optoelectron. Adv. Mater. **7**, 2625–2634 (2005).
8. K. Michel, B. Bureau, C. Boussard-Plédel, T. Jouan, J. L. Adam, K. Staubmann, and T. Baumann, "Monitoring of pollutant in waste water by infrared spectroscopy using chalcogenide glass optical fibers," Sens. Actuators B. Chem. **101**, 252–259 (2004).
9. J. Keirsse, C. Boussard-Pledel, O. Loreal, O. Sire, B. Bureau, B. Turlin, P. Leroyer, and J. Lucas, "Chalcogenide glass fibers used as biosensors," J. Non-Cryst. Solids **326**, 430–433 (2003).
10. S. Ramachandran and S. G. Bishop, "Photoinduced integrated-optic devices in rapid thermally annealed chalcogenide

glasses," IEEE J. Sel. Top. Quantum Electron. **11**, 260–270 (2005).

11. D. A. Turnbull, J. S. Sanghera, V. Nguyen, and I. D. Aggarwal, "Fabrication of waveguides in sputtered films of GeAsSe glass via photodarkening with above bandgap light," Mater. Lett. **58**, 51–54 (2004).

12. A. Saliminia, A. Villeneuve, T. V. Galstyan, S. LaRochelle, and K. Richardson, "First- and second-order Bragg gratings in single-mode planar waveguides of chalcogenide glasses," J. Lightwave Technol. **17**, 837–842 (1999).

13. N. J. Baker, H. W. Lee, I. C. M. Littler, C. M. de Sterke, B. J. Eggleton, D. Y. Choi, S. Madden, and B. Luther-Davies, "Sampled Bragg gratings in chalcogenide (As2S3) rib-waveguides," Opt. Express **14**, 9451–9459 (2006).

14. J. Lumeau, M. Lequime, C. Amra, N. Kaiser, and H. A. Macleod, "Laser trimming of thin-film filters," Proc. SPIE **5963**, 60–69 (2005).

15. T. K. Sudoh, Y. Nakano, and K. Tada, "Wavelength trimming by external light irradiation-post-fabrication lasing wavelength adjustment for multiple-wavelength distributed-feedback laser arrays," IEEE J. Sel. Top. Quantum Electron. **3,** 577–583 (1997).

16. M. Frumar, H. Ticha, M. Vlcek, J. Klikorka, and L. Tichy, "Photostructural changes in some ternary Ge–Sb–S chalcogenide layers," Czech. J. Physics **31**, 441–446 (1981).

17. M. Frumar, B. Frumarova, P. Nemec, T. Wagner, J. Jedelsky, and M. Hrdlicka, "Thin chalcogenide films prepared by pulsed laser deposition—new amorphous materials applicable in optoelectronics and chemical sensors," J. Non-Cryst. Solids **352,** 544–561 (2006).

18. H. A. Macleod and E. Pelletier, "Error compensation mechanisms in some thin-film monitoring system," J. Mod. Opt. **24,** 907–930 (1977).

19. B. Vidal, A. Fornier, and E. Pelletier, "Optical monitoring of nonquarterwave multilayer filters," Appl. Opt. **17**, 1038–1047 (1978).

20. C. Deumié, R. Richier, P. Dumas, and C. Amra, "Multiscale roughness in optical multilayers: atomic force microscopy and light scattering," Appl. Opt. **35**, 5583–5594 (1996).

21. L. Abel-Tiberini, F. Lemarquis, and M. Lequime, "Dedicated spectrophotometer for localized transmittance and reflectance measurements," Appl. Opt. **45**, 1386–1391 (2006).

22. V. Nazabal, P. Nemec, J. Jedelsky, C. Duverger, J. Le Person, J. L. Adam, and M. Frumar, "Dysprosium doped amorphous chalcogenide films prepared by pulsed laser deposition," Opt. Mater. **29**, 273–278 (2006).

23. J. P. Borgogno, B. Lazarides, and E. Pelletier, "Automatic determination of the optical constants of inhomogeneous thin films," Appl. Opt. **21**, 4020–4029 (1982).

24. B. Bovard, F. J. Van Milligen, M. J. Messerly, S. J. Saxe, and H. A. Macleod, "Optical constants derivation for an inhomogeneous thin film from *in situ* transmission measurements," Appl. Opt. **24**, 1803–1807 (1985).

25. P. K. Tien, R. Ulrich, and R. J. Martin, "Modes of propagating light waves in thin deposited semiconductor films," Appl. Phys. Lett. **14**, 291–294 (1969).

26. R. Ulrich and R. Torge, "Measurement of thin film parameters with a prism coupler," Appl. Opt. **12**, 2901–2908 (1973).

27. J. M. Bennett, E. Pelletier, G. Albrand, J.-P. Borgogno, B. Lazarides, C. K. Carniglia, R. A. Schmell, T. H. Allen, T. Tuttle-Hart, K. H. Guenther, and C. Saxer, "Comparison of the properties of titanium dioxide films prepared by various techniques," Appl. Opt. **28**, 3303–3317 (1989).

28. M. Frumar, J. Jedelsky, B. Frumarov, T. Wagner, and M. Hrdlicka, "Optically and thermally induced changes of structure, linear and non-linear optical properties of chalcogenides thin films," J. Non-Cryst. Solids **326 & 327**, 399–404 (2003).

29. G. Lucovsky, F. L. Galeener, R. C. Keezer, R. H. Geils, and H. A. Six, "Structural interpretation of the infrared and Raman spectroscopy of glasses in the alloy system $Ge_{1-x}S_x$," Phys. Rev. B **10**, 5134–5146 (1974).

30. I. Watanabe, S. Noguchi, and T. Shimizu, "Study on local structure in amorphous Sb–S films by Raman scattering," J. Non-Cryst. Solids **58**, 35–40 (1983).

31. I. P. Kotsalas, D. Papadimitriou, C. Raptis, M. Vlcek, and M. Frumar, "Raman study of photostructural changes in amorphous $Ge_xSb_{0.4-x}S_{0.6}$," J. Non-Cryst. Solids **226**, 85–91 (1998).

32. S. Sugai, "Stochastic random network model in ge and Si chalcogenide glasses," Phys. Rev. B **35**, 1345–1361 (1987).

33. A. T. Ward, "Raman spectroscopy of sulfur, sulfur-selenium, and sulfur-arsenic mixtures," J. Phys. Chem. **72**, 4133–4139 (1968).

34. T. Mori, S. Onari, and T. Arai, "Raman scattering in amorphous As–Se system," Jpn. J. Appl. Phys. **19**, 1027–1031 (1980).

35. J. Schottomiller, M. Tabak, G. Lukovsky, and A. Ward, "The effects of valency on transport properties in vitreous binary alloys of selenium," J. Non-Cryst. Solids **4**, 80–96 (1970).

36. A. Mendoza-Galvan, E. Garcia-Garcia, Y. V. Vorobiev, and J. Gonzalez-Hernandez, "Structural, optical and electrical characterization of amorphous SeTe thin film alloys," Microelectron. Eng. **51–52,** 677–687 (2000).

37. T. Usuki, K. Saitoh, M. Endo, and O. Uemura, "Short-range order of amorphous and liquid As–Te–I system," J. Non-Cryst. Solids **205–207**, 184–188 (1996).

38. K. H. Guenther, B. Loo, D. Burns, J. Edgell, D. Windham, and K. H. Müller, "Microstructure analysis of thin films deposited by reactive evaporation and reactive ion plating," J. Vac. Sci. Technol. **A7**, 1436–1445 (1989).

39. P. J. S. Ewen, A. Zekak, C. W. Slinger, G. Dale, D. A. Pain, and A. E. Owen, "Diffractive infrared optical-elements in chalcogenide glasses," J. Non-Cryst. Solids **166**, 1247–1250 (1993).

40. M. A. Popescu, *Noncrystalline Chalcogenides* (Kluwer, 2000).

41. Y. L. Ruan, W. T. Li, R. Jarvis, N. Madsen, A. Rode, and B. Luther-Davies, "Fabrication and characterization of low loss rib chalcogenide waveguides made by dry etching," Opt. Express **12**, 5140–5145 (2004).

42. C. Vigreux-Bercovici, E. Bonhomme, A. Pradel, J. E. Broquin, L. Labadie, and P. Kern, "Transmission measurement at 10.6 μm of $Te_2As_3Se_5$ rib waveguides on As_2S_3 substrate," Appl. Phys. Lett. **90**, 011110 (2007).

43. M. L. Anne, V. Nazabal, V. Moizan, C. Boussard-Pledel, B. Bureau, J. L. Adam, P. Nemec, M. Frumar, A. Moreac, H. Lhermite, P. Camy, J. L. Doualan, J. P. Guin, J. Le Person, F. Colas, C. Compere, M. Lehaitre, F. Henrio, D. Bosc, J. Charrier, A.-M. Jurdyc, and B. Jacquier, "Chalcogenide waveguide for IR optical range," Proc. SPIE **6475**, 647508 (2007).